

Spherical Needlets for CMB Data Analysis

D. Marinucci^{1*}, D. Pietrobon², A. Balbi^{2,3}, P. Baldi¹, P. Cabella⁴,
G. Kerkycharian⁵, P. Natoli^{2,3}, D. Picard⁶, N. Vittorio^{2,3}

¹ *Dipartimento di Matematica, Università di Roma “Tor Vergata”, Via della Ricerca Scientifica 1, 00133 Roma*

² *Dipartimento di Fisica, Università di Roma “Tor Vergata”, Via della Ricerca Scientifica 1, 00133 Roma*

³ *INFN Sezione di Roma “Tor Vergata”, Via della Ricerca Scientifica 1, 00133 Roma*

⁴ *University of Oxford, Astrophysics, Keble Road, Oxford, OX1 3RH, U.K.*

⁵ *Université de Paris 10 and Laboratoire de Probabilités et Modèles Aléatoires*

⁶ *Université de Paris 7 and Laboratoire de Probabilités et Modèles Aléatoires*

28 May 2018

ABSTRACT

We discuss Spherical Needlets and their properties. Needlets are a form of spherical wavelets which do not rely on any kind of tangent plane approximation and enjoy good localization properties in both pixel and harmonic space; moreover needlets coefficients are asymptotically uncorrelated at any fixed angular distance, which makes their use in statistical procedures very promising. In view of these properties, we believe needlets may turn out to be especially useful in the analysis of Cosmic Microwave Background (CMB) data on the incomplete sky, as well as of other cosmological observations. As a final advantage, we stress that the implementation of needlets is computationally very convenient and may rely completely on standard data analysis packages such as HEALPIX.

Key words: methods: data analysis, cosmology: observations, cosmic microwave background

1 INTRODUCTION

Over the last few years, wavelets have emerged as one of the most powerful tools of CMB data analysis, finding applications in virtually all areas where statistical methods are required; a very incomplete list of references should include testing for non-Gaussianity (see Vielva et al. (2004); Cabella et al. (2004)), foreground subtraction (Hansen et al. (2006)), point source detection (Sanz et al. (2006)), component separation (Moudden et al. (2005); Starck et al. (2006)), polarization analysis (Cabella et al. (2007)) and many others. The reason for such a strong interest is easily understood. As it is well-known, CMB models are best analyzed in the frequency domain, where the behaviour at different multipoles can be investigated separately; on the other hand, partial sky coverage and other missing observations make the evaluation of exact spherical harmonic transforms troublesome. The combination of these two features makes the time-frequency localization properties of wavelets most valuable.

Despite the wide agreement on their importance as a data analysis instrument, the derivation of an optimal wavelets basis on the sphere is still an open issue for re-

search. Many efforts have been undertaken in this area, most of them being based upon the so-called tangent plane approach (Antoine & Vanderghenst 1999). In this framework, a flat sky approximation is entertained locally, and then some form of standard plane wavelets are implemented. Directional wavelets have been advocated by McEwen et al. (2006, 2007), again by means of a tangent plane approximation. An interesting attempt to overcome the tangent plane approximation is due to Sanz et al. (2006).

A new approach to spherical wavelets was introduced in the statistical literature by Baldi et al. (2006), adapting tools proposed in the functional analysis literature by Narcowich et al. (2006); the first application to CMB data is due to Pietrobon et al. (2006), (see also Guilloux et al. (2007); Baldi et al. (2007)). The idea is to focus on so-called needlets, to be described in the following section. Needlets enjoy several features which are not in general granted by other spherical wavelets construction; we anticipate some of these features, which we shall investigate more deeply in the Sections to come. More precisely:

a) they do not rely on any tangent plane approximation (compare Sanz et al. 2006), and take advantage of the manifold structure of the sphere;

b) being defined in harmonic space, they are computa-

* E-mail: marinucc@mat.uniroma2.it

tionally very convenient, and natively adapted to standard packages such as HEALPix¹ (Górski et al. 2005);

c) they allow for a simple reconstruction formula (see Eq. 5), where the same needlets functions appear both in the direct and the inverse transform (see also Kerkyacharian et al. 2007). This property is the same as for spherical harmonics but it is *not* shared by other wavelets systems such as the well-known Spherical Mexican Hat Wavelets (hereafter SMHW);

d) they are quasi-exponentially (i.e. faster than any polynomial) concentrated in pixel space, see Eq. 6 below;

e) they are exactly localized on a finite number of multipoles; the width of this support is explicitly known and can be specified as an input parameter (see Eq. 1);

f) random needlets coefficients can be shown to be asymptotically uncorrelated (and hence, in the Gaussian case, independent) at any fixed angular distance, when the frequency increases. This capital property can be exploited in several statistical procedures, as it allows to treat needlets coefficients as a sample of independent and identically distributed coefficients on small scales, at least under the Gaussian assumption.

The aim of this paper is to discuss more thoroughly the implementation of needlets, compare it with other wavelets (namely, the SMHW) and investigate their properties by means of Monte Carlo simulations. In Section 2 we describe the numerical implementation, taking care to discuss the features of the construction that ensure the above-mentioned properties. In Section 3 we discuss the relationship between the localization properties in frequency and pixel spaces; we also discuss the trade-off between the two, which from the operational point of view relates to the issue of an optimal choice of a so-called “bandwidth” parameter B . Some comparisons are made with existing techniques to deal with partial sky coverage, and more precisely with tophat binning procedures and SMHW. Some discussion on possible applications and directions for further research is collected in Section 4.

2 THE NUMERICAL IMPLEMENTATION OF NEEDLETS

We start by outlining briefly the construction of a needlets basis. More details can be found in Narcowich et al. (2006), and in Baldi et al. (2006). We shall discuss the details of the construction step by step, in order to provide to potential users a clear recipe for needlets implementation.

We first recall that the spherical needlet (function) is defined as

$$\psi_{jk}(\hat{\gamma}) = \sqrt{\lambda_{jk}} \sum_{\ell} b\left(\frac{\ell}{B^j}\right) \sum_{m=-\ell}^{\ell} \bar{Y}_{\ell m}(\hat{\gamma}) Y_{\ell m}(\xi_{jk}); \quad (1)$$

here, we use $\{\xi_{jk}\}$ to denote a set of *cubature points* on the sphere, corresponding to frequency j ; in practice, we shall identify these points with the pixel centres in HEALPix. Also, λ_{jk} denotes the cubature weights, which for simplicity can be envisaged as $1/N_p$, N_p denoting the number of pixels (see Pietrobon et al. 2006).

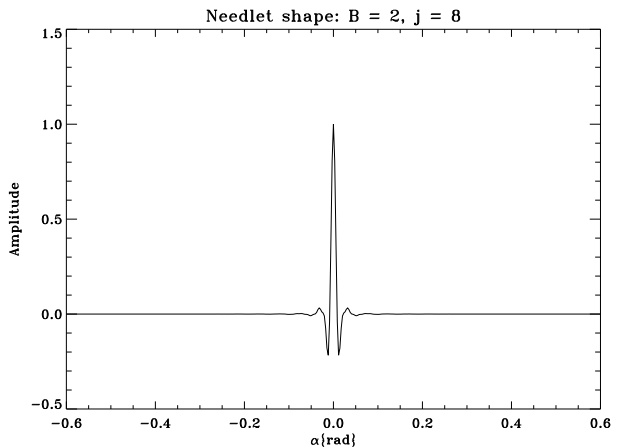


Figure 1. Needlets in pixel space. $B = 2$, $j = 8$

Intuitively, needlets should be viewed as a convolution of the projection operator $\sum_{m=-\ell}^{\ell} \bar{Y}_{\ell m}(\hat{\gamma}) Y_{\ell m}(\xi_{jk})$ with a suitably chosen window function $b(\cdot)$. Special properties of $b(\cdot)$ ensure that the needlets enjoy quasi-exponential localization properties in pixel space. Formally, we must ensure that (Narcowich et al. 2006; Baldi et al. 2006):

- (i) $b^2(\cdot)$ has support in $[\frac{1}{B}, B]$, and hence $b(\frac{\ell}{B^j})$ has support in $\ell \in [B^{j-1}, B^{j+1}]$
- (ii) the function $b(\cdot)$ is infinitely differentiable in $(0, \infty)$.
- (iii) we have

$$\sum_{j=1}^{\infty} b^2\left(\frac{\ell}{B^j}\right) \equiv 1 \text{ for all } \ell > B. \quad (2)$$

It is immediate to see that property (i) ensures the needlets have bounded support in the harmonic domain; property (ii) is the crucial element in the derivation of the localization properties, which we shall illustrate in the following section. Finally, property (iii) is necessary to establish the reconstruction formula which we shall discuss below; functions such as $b^2(\cdot)$ are called *partitions of unity*.

There are of course many possible constructions satisfying (i-iii); indeed an interesting theme for future research is the derivation of optimal windows satisfying these three conditions (compare Guilloux et al. 2007). An explicit recipe for the construction of $b(\cdot)$ is as follows.

STEP 1: Construct the function

$$f(t) = \begin{cases} \exp\left(-\frac{1}{1-t^2}\right), & -1 \leq t \leq 1 \\ 0, & \text{otherwise} \end{cases}.$$

It is immediate to check that the function $f(\cdot)$ is C^∞ and compactly supported in the interval $(-1, 1)$

STEP 2: Construct the function

$$\psi(u) = \frac{\int_{-1}^u f(t) dt}{\int_{-1}^1 f(t) dt}.$$

The function $\psi(\cdot)$ is again C^∞ ; it is moreover non-decreasing and normalized so that $\psi(-1) = 0$, $\psi(1) = 1$

STEP 3: Construct the function

¹ <http://healpix.jpl.nasa.gov>

$$\varphi(t) = \begin{cases} 1 & \text{if } 0 \leq t \leq \frac{1}{B} \\ \psi(1 - \frac{2B}{B-1}(t - \frac{1}{B})) & \text{if } \frac{1}{B} \leq t \leq 1 \\ 0 & \text{if } t > 1 \end{cases}$$

Here we are simply implementing a change of variable so that the resulting function $\varphi(\cdot)$ is constant on $(0, B^{-1})$ and monotonically decreasing to zero in the interval $(B^{-1}, 1)$. Indeed it can be checked that

$$1 - \frac{2B}{B-1}(t - \frac{1}{B}) = \begin{cases} 1 & \text{for } t = \frac{1}{B} \\ -1 & \text{for } t = 1 \end{cases}$$

and

$$\begin{aligned} \varphi(\frac{1}{B}) &= \psi(1) = 1 \\ \varphi(1) &= \psi(-1) = 0 \end{aligned}$$

STEP 4: Construct

$$b^2(\xi) = \varphi(\frac{\xi}{B}) - \varphi(\xi)$$

The expression for $b^2(\cdot)$ is meant to ensure that the function satisfies the partition-of-unity property of Eq. 2. Needless to say, for $b(\xi) = \{\varphi(\frac{\xi}{B}) - \varphi(\xi)\}^{1/2}$ we take the positive root.

Random needlets coefficients are hence given by

$$\begin{aligned} \beta_{jk} &= \int_{S^2} T(\hat{\gamma}) \psi_{jk}(\hat{\gamma}) d\Omega \\ &= \sqrt{\lambda_{jk}} \sum_{\ell} b(\frac{\ell}{B^j}) \sum_{m=-\ell}^{\ell} \left\{ \int_{S^2} T(\hat{\gamma}) \bar{Y}_{\ell m}(\hat{\gamma}) d\Omega \right\} Y_{\ell m}(\xi_{jk}) \\ &= \sqrt{\lambda_{jk}} \sum_{\ell} b(\frac{\ell}{B^j}) \sum_{m=-\ell}^{\ell} a_{\ell m} Y_{\ell m}(\xi_{jk}). \end{aligned} \quad (3)$$

It is very important to stress that, although the needlets do *not* make up an orthonormal basis for square integrable functions on the sphere, they do represent a *tight frame*. In general, a tight frame on the sphere is a countable set of functions $\{e_j\}$ such that, for all square integrable functions on the sphere $f \in L^2(S^2)$, we have

$$\sum_j \langle f, e_j \rangle^2 \equiv \int_{S^2} f(\hat{\gamma})^2 d\Omega,$$

so that the norm is preserved. Of course, this norm-preserving property is shared by all orthonormal systems; however, frames do not in general make up a basis, as they admit redundant elements. They can be viewed as the closer system to a basis, for a given redundancy, see Hernández & Weiss (1996), Baldi et al. (2006) for further definitions and discussion. In our framework, the norm-preserving property becomes

$$\sum_{j,k} \hat{\beta}_{jk}^2 \equiv \sum_{\ell=1}^{\infty} \frac{2\ell+1}{4\pi} \hat{C}_{\ell}, \quad (4)$$

where

$$\hat{C}_{\ell} = \frac{1}{2\ell+1} \sum_m |a_{\ell m}|^2$$

is the raw angular power spectrum of the map $T(\hat{\gamma})$. The

identity in Eq. 4 has indeed been verified by means of numerical simulations and implicitly provides the correct normalization for needlets. It is basically a consequence of the peculiar partition-of-unity property of $b(\cdot)$ of Eq. 2. Of course this property is not generally shared by other constructions such as SMHW, where the wavelets functions are normalized to unity in the real domain. Eq. 4 is related to a much more fundamental result, i.e. the reconstruction formula

$$T(\hat{\gamma}) \equiv \sum_{j,k} \beta_{jk} \psi_{jk}(\hat{\gamma}) \quad (5)$$

which in turn is a non-trivial consequence of the careful construction leading to Eq. 2. As mentioned before, the simple reconstruction formula of Eq. 5 is typical of tight frames but does not hold in general for other wavelets systems. It is easy to envisage many possible applications of this result when handling masked data.

3 PROPERTIES AND COMPARISONS

The following quasi-exponential localization property of needlets is due to Narcowich et al. (2006) and motivates their name.

For any $k = 1, 2, \dots$ there exists a positive constant c_k such that for any point $\hat{\gamma} \in S^2$ we have

$$|\psi_{jk}(\hat{\gamma})| \leq \frac{c_k B^j}{(1 + B^j \arccos(\langle \hat{\gamma}, \xi_{jk} \rangle))^k}. \quad (6)$$

We recall that $\arccos(\langle \hat{\gamma}, \xi_{jk} \rangle)$ is just the natural distance on the unit sphere between the points $(\hat{\gamma}, \xi_{jk})$. The meaning of Eq. 6 is then clear: for any fixed angular distance, the value of $\psi_{jk}(\hat{\gamma})$ goes to zero quasi-exponentially in the parameter B . The resulting trade-off in the behaviour over the harmonic and real spaces is expected: smaller values of B correspond to a tighter localization in harmonic space (less multipoles entering into any needlet), whereas larger values ensure a faster decay in real space.

Due to their localization properties, needlets are especially useful in the analysis of partial sky coverage. In fact, in view of Eq. 6 we expect the value of needlets coefficients to be mildly affected by the presence of gaps in the maps. To illustrate this important feature, we plot the quantity

$$\chi_{jk} = \frac{\langle (\beta_{jk,mask} - \beta_{jk})^2 \rangle}{\langle \beta_{jk}^2 \rangle} \quad (7)$$

in Fig. 2, where the Kp0 mask², that is used to remove Galactic emission and point sources from WMAP data (roughly 75% of the sky), is applied. The expected values of Eq. 7 are again evaluated by means of 100 Monte Carlo simulations; in particular we focus on needlets coefficients corresponding to $B = 2.72$ and $j = 5$, which amounts to a range in multipoles space in the order of $58 < \ell < 398$. To put our results in perspective, in the same Figure we show analogous findings with the use of a tophat binning filter and SMHW. We remind the SMHW formula

$$\Psi(y, R) = \frac{1}{\sqrt{2\pi}N(R)} \left[1 + \left(\frac{y}{2} \right)^2 \right]^{-2} \times$$

² See LAMBDA website, <http://lambda.gsfc.nasa.gov/>

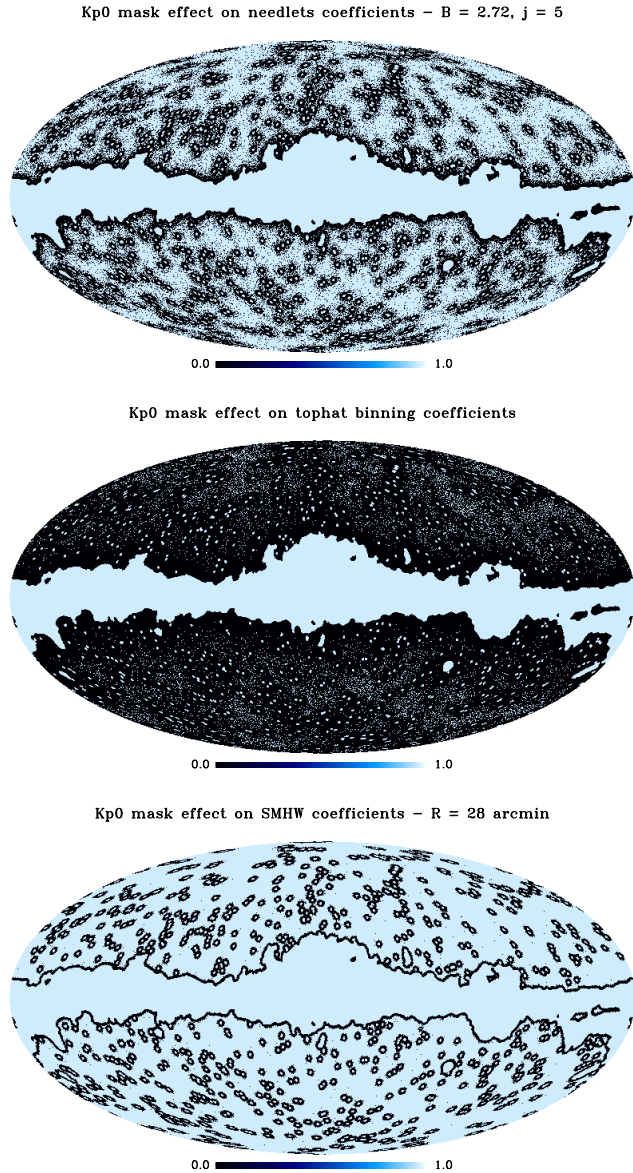


Figure 2. Effect of incomplete sky coverage, modeled by the WMAP Kp0 mask, visualized by plotting on a sky map the quantity defined in Eq. 7. From top to bottom, the result for needlets, flat binning, and SMHW (28').

$$\times \left[2 - \left(\frac{y}{R} \right)^2 \exp(-y^2/2R^2) \right]$$

where $y = 2 \tan \theta / 2$ (θ is the polar angle), R is the scale of convolution and $N(R)$ a normalization factor (Martínez-González et al. 2002).

Under these circumstances, needlets coefficients are well localized, but slightly sensitive to the mask. Indeed, only 56% of the pixel are changed by less than 0.1; SMHW coefficients perform a bit better (73%) while a simple tophat binning fails completely (only 6%). The difference between the two wavelets bases can be due to the different power that they give to multipoles (see Fig. 4). In fact the performance of needlets can be improved choosing the appropriate B^j , that defines the optimal shape for the window $b(\cdot)$, given the

multipoles range of interest. For details see Guilloux et al. (2007). In the same paper, the authors argue that an optimal filter can be adapted to deconvolve a specific mask: this property provides a further degree of flexibility to the needlets toolbox.

In Baldi et al. (2006), another relevant property of needlets coefficients was discussed, namely their asymptotic uncorrelation at any fixed angular distance, for growing frequencies j . More explicitly, at high frequency needlets coefficients can be approximated as a sample of identically distributed and independent (under Gaussianity) coefficients, and this property opens the way to a huge toolbox of statistical procedures for CMB data analysis (for instance, for testing Gaussianity and isotropy). Also, in view of Eq. 3, for full sky maps and in the absence of any mask we should expect the theoretical correlation to be identically zero whenever $|j_1 - j_2| \geq 2$.

Let us define the realized correlation between two different scales j_1, j_2 as

$$\rho_{j_1 j_2} = \frac{\sum_k \langle \beta_{j_1 k} \beta_{j_2 k} \rangle}{\sqrt{\sum_k \langle \beta_{j_1 k}^2 \rangle \sum_k \langle \beta_{j_2 k}^2 \rangle}}. \quad (8)$$

By using Eq. 3 one has that:

$$\langle \beta_{j_1 k} \beta_{j_2 k} \rangle = \sum_{\ell} b(\ell/B^{j_1}) b(\ell/B^{j_2}) C_{\ell} \sum_m K_{\ell m m m}$$

where C_{ℓ} is the underlying CMB angular power spectrum and the coupling kernel $K_{\ell \ell' m m'}$ is defined in terms of the observed mask $W(\hat{\gamma})$ (see e.g. Hivon et al. 2002):

$$K_{\ell \ell' m m'} = \int_{S^2} Y_{\ell m}(\hat{\gamma}) Y_{\ell' m'}(\hat{\gamma}) W(\hat{\gamma}) d\Omega$$

Note that, in the absence of gaps (i.e. $W(\hat{\gamma}) = 1$), $\sum_m K_{\ell \ell m m}$ reduces simply to $(2\ell + 1)$.

Equation (8) can not be expected to be reproduced exactly, due to numerical approximations; in particular, we should stress that theoretical results are derived under the assumption that needlets coefficients are evaluated at *exact* cubature points, so that the $\{a_{\ell m}\}$ are precisely reconstructed from the maps. Of course, this is not the case in practice; however, we do expect small and vanishing values for $j_1 \ll j_2$. At the same time, we expect this correlation to increase on the presence of sky cuts, but less so than for other bases. Here, we want to illustrate the practical relevance of this mathematical results by means of simulations on the correlation coefficient. More precisely, we computed the quantity (8) by performing a Monte Carlo over 100 simulations. Our findings are shown in Tables 1, 2.

We view these results as very encouraging. In the absence of a mask, the correlation coefficient is by any practical means virtually negligible for all frequency distances greater or equal than 2, while at distance $\Delta j = 1$ the correlation is around ~ 0.25 in good agreement with eqn. 8 which predicts 0.22 for our input parameters. In the presence of sky cuts, the performance deteriorates as expected only at low j where it exceeds a few percentage points, as shown for our simulations in the case of the Kp0 mask. A computation analogous to (8) yields for SMHW the theoretical results reported in Table 3; note how we have non zero values at all lags. Numerical results to support the theoretical findings are provided by Tables 4, 5. We believe these compared

Table 1. Needlets correlation parameter. $B = 2.72$ without gaps

j/j'	1	2	3	4	5
1	1.000	0.275	0.001	0.001	0.003
2	-	1.000	0.248	0.001	0.001
3	-	-	1.000	0.268	0.001
4	-	-	-	1.000	0.242
5	-	-	-	-	1.000

Table 2. Needlets correlation parameter. $B = 2.72$ with gaps

j/j'	1	2	3	4	5
1	1.000	0.420	0.140	0.040	0.060
2	-	1.000	0.335	0.023	0.001
3	-	-	1.000	0.291	0.004
4	-	-	-	1.000	0.252
5	-	-	-	-	1.000

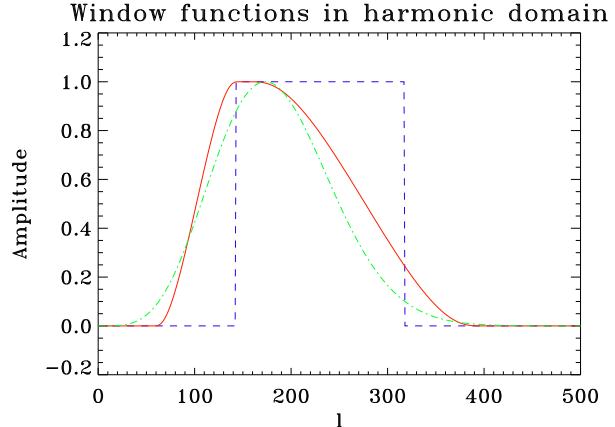
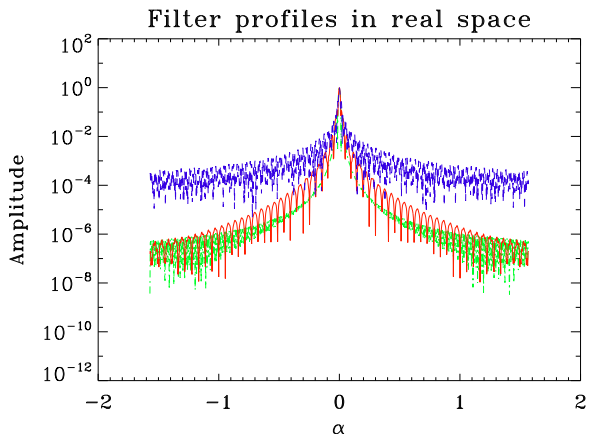
results strongly support the potential of needlets for the implementations of statistical procedures, where uncorrelation properties are clearly a very valuable asset.

As a further comparison, we evaluated the domains in harmonic and real spaces for needlets, tophat binning and SMHW. In particular we normalized the three bases to have roughly an equal area in the harmonic domain, paying attention to have the maximum of the power in a similar range of multipoles. Results are plotted in Fig. 4, 5. It is evident how SMHW and needlets outperform tophat binning by two order of magnitudes in terms of localization in real space: indeed in this domain the two wavelets constructions perform quite similarly. Moreover, in Figure 7, we computed the angle where the integral of the filter functions in pixel space reaches 68%, 95% and 99% of the total area, respectively. Again, it is immediate to check how at every scale needlets outperform very clearly a simple binning approach; on the other hand, SMHW seems slightly more concentrated in this setting. The linear trend for needlets in the log-log plot is a direct consequence of their construction, and in particular of the functional dependence on ℓ/B^j .

On the other hand the advantage of needlets over SMHW emerges quite clearly in the harmonic domain. More precisely, after normalizing the two methods to be centred at the same angular scale, with roughly the same total power, the needlets support seems clearly more concentrated than SMHW. In particular we stress how SMHW suffer from

Table 3. Theoretical correlation (full sky) for needlets and SMHW

corr/ Δj	0	1	2	3	4
Needlets	1.000	0.220	0.000	0.000	0.000
SMHW	1.000	0.500	0.100	0.014	0.002

**Figure 4.** The red solid line represents needlets window function, $b(\frac{\ell}{B^j})$ in harmonic space for $B = 2.72$, $j = 5$. The blue dashed and green dot-dashed lines provide the tophat and the SMHW window functions, respectively. The SMHW corresponds to a scale $R = 28'$ in pixel space.**Figure 5.** Behaviour of needlets (solid red), SMHW (dot-dashed green) and tophat binning (blue dashed) in pixel space. The angle in horizontal axis is measured in radians.

“leakage” by the very low multipoles, i.e. exactly those most affected by sky cuts and cosmic variance. No such leakage occurs for needlets.

4 CONCLUDING REMARKS

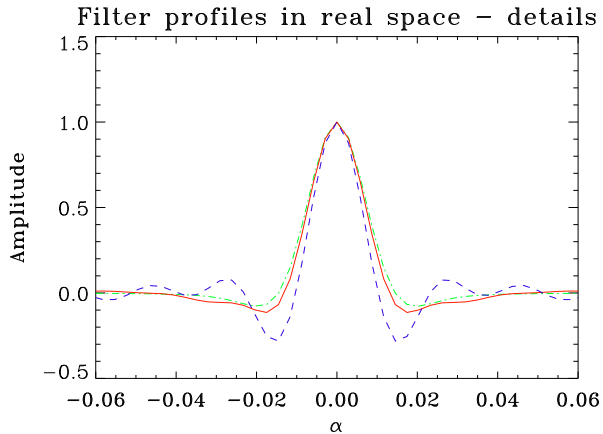
In this paper, we have described a new construction for a spherical wavelets frame, and we have illustrated several of its properties; most notably localization properties in the real and harmonic spaces, uncorrelations of the resulting random coefficients, and independence from any tangent plane approximations. Moreover, needlets enjoy a direct reconstruction property which allows analysis and synthesis to be implemented directly and in a computationally convenient manner. Each of these properties has been illustrated by means of Monte Carlo simulations. The encouraging results reported suggest that needlets can become a valuable

Table 4. SMHW correlation parameter without gaps. The scale R is given in arcmin.

R/R'	1792	896	448	224	112	56	28
1792	1.000	0.503	0.109	0.016	0.002	0.0002	0.00003
896	-	1.000	0.500	0.099	0.014	0.002	0.0002
448	-	-	1.000	0.510	0.103	0.014	0.002
224	-	-	-	1.000	0.511	0.104	0.014
112	-	-	-	-	1.000	0.513	0.107
56	-	-	-	-	-	1.000	0.519
28	-	-	-	-	-	-	1.000

Table 5. SMHW correlation parameter with gaps. The scale R is given in arcmin.

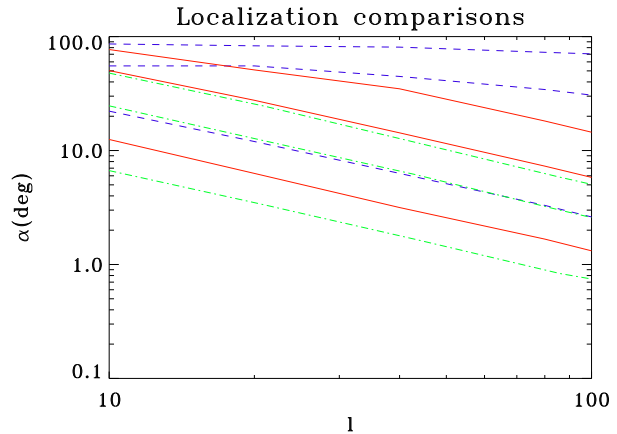
R/R'	1792	896	448	224	112	56	28
1792	1.000	0.496	0.113	0.022	0.005	0.002	0.0007
896	-	1.000	0.520	0.115	0.021	0.005	0.002
448	-	-	1.000	0.523	0.114	0.021	0.005
224	-	-	-	1.000	0.520	0.114	0.020
112	-	-	-	-	1.000	0.522	0.116
56	-	-	-	-	-	1.000	0.527
28	-	-	-	-	-	-	1.000

**Figure 6.** Here in this figure we provide details of the behaviour in pixel space over the relevant range, i.e. the region where the three functions exceed 0.001. Lines have the same meaning as in the previous figures.

tool in the several areas of CMB data analysis where other wavelets have already proved useful.

ACKNOWLEDGMENTS

Some of the results in this paper have been derived using the HEALPix (Górski et al., 2005) package.

**Figure 7.** The three lines represent the angle at which the area of needlet, in red, or the tophat, in blue, filter reaches the 99%, 95%, 68% of the total area as a function of the peak multipole in each window function. The latter corresponds directly to a given j for needlets and to the scale R for SMHW; for the tophat window the central ℓ in the band is taken.

REFERENCES

- Antoine J.-P., Vandergheynst P., 1999, Appl. Comput. Harmon. Anal., 7, 262
 Baldi P., Kerkyacharian G., Marinucci D., Picard D., 2006, Under revision for the Annals of Statistics, arXiv:math.ST/0606599

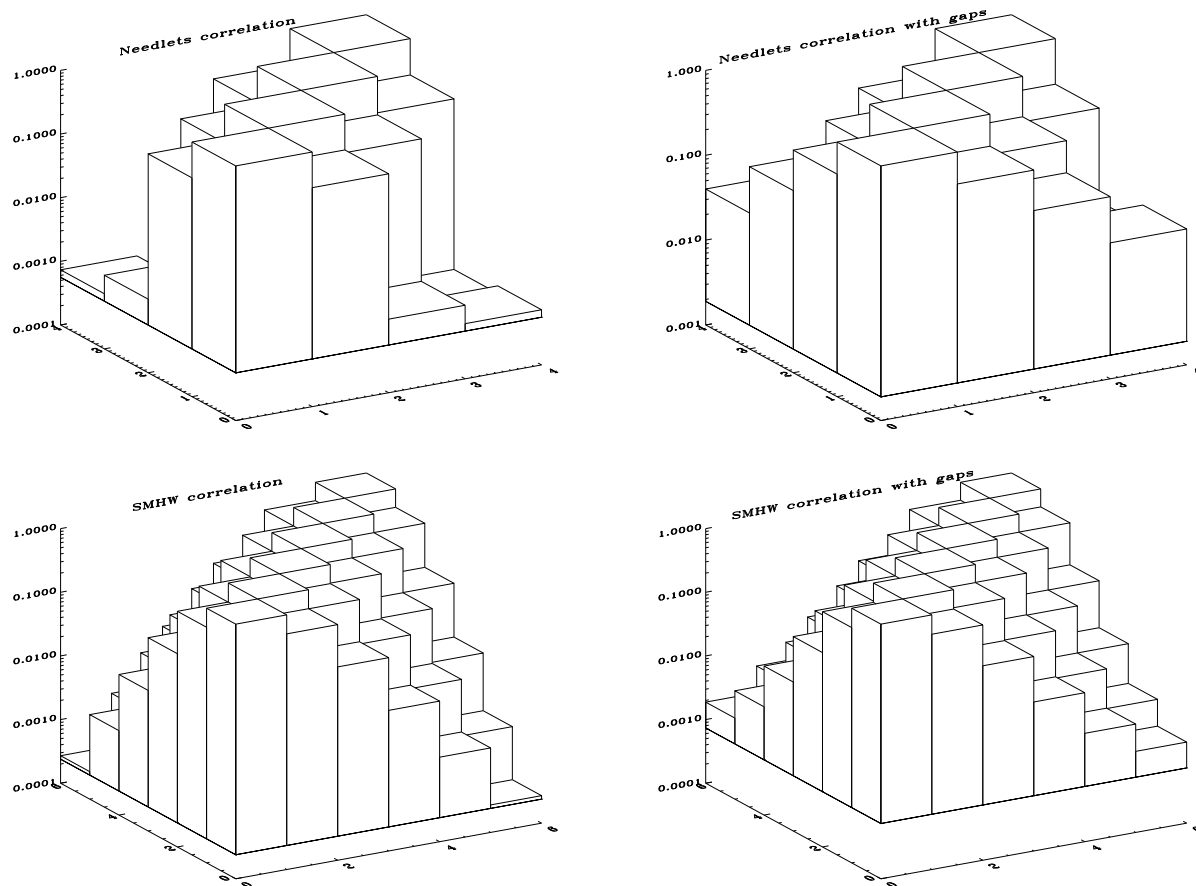


Figure 3. The correlation for needlets (top panels) and SMHW (bottom panels) is plotted as a function of the scale, in absence (left panels) and in presence (right panel) of sky cuts (Kp0 mask).

Baldi P., Kerkyacharian G., Marinucci D., Picard D., 2007, ArXiv e-prints, 706, 0706.4169

Cabella P., Hansen F., Marinucci D., Pagano D., Vittorio N., 2004, Phys. Rev. D, 69, 063007, arXiv:astro-ph/0401307

Cabella P., Natoli P., Silk J., 2007, ArXiv e-prints, 705, 0705.0810

Górski K. M., Hivon E., Banday A. J., Wandelt B. D., Hansen F. K., Reinecke M., Bartelmann M., 2005, ApJ, 622, 759, arXiv:astro-ph/0409513

Guiloux F., Fay G., Cardoso J.-F., 2007, ArXiv e-prints, 706, 0706.2598

Hansen F. K., Banday A. J., Eriksen H. K., Górski K. M., Lilje P. B., 2006, ApJ, 648, 784, arXiv:astro-ph/0603308

Hernández E., Weiss G., 1996, A first course on wavelets, Studies in Advanced Mathematics. CRC Press, Boca Raton, FL, pp. xx+489, with a foreword by Yves Meyer

Hivon E., Górski K. M., Netterfield C. B., Crill B. P., Prunet S., Hansen F., 2002, ApJ, 567, 2, arXiv:astro-ph/0105302

Kerkyacharian G., Petrushev P., Picard D., Willer T., 2007, Electronic Journal of Statistics, 1, 30

Martínez-González E., Gallegos J. E., Argüeso F., Cayón L., Sanz J. L., 2002, MNRAS, 336, 22, arXiv:astro-ph/0111284

McEwen J. D., Hobson M. P., Lasenby A. N., Mortlock

D. J., 2006, MNRAS, 371, L50, arXiv:astro-ph/0604305

McEwen J. D., Vielva P., Hobson M. P., Martínez-González E., Lasenby A. N., 2007, MNRAS, 376, 1211, arXiv:astro-ph/0602398

Moudden Y., Cardoso J. ., Starck J. ., Delabrouille J., 2005, EURASIP Journal of Applied Signal Processing, 15, 2437, astro-ph/0407053

Narcowich F. J., Petrushev P., Ward J. D., 2006, SIAM J. Math. Anal., 38, 574

Pietrobon D., Balbi A., Marinucci D., 2006, Phys. Rev. D, 74, 043524, arXiv:astro-ph/0606475

Sanz J. L., Herranz D., Lopez-Caniego M., Argüeso F., 2006, ArXiv Astrophysics e-prints, astro-ph/0609351

Starck J.-L., Moudden Y., Abrial P., Nguyen M., 2006, A&A, 446, 1191, arXiv:astro-ph/0509883

Vielva P., Martínez-González E., Barreiro R. B., Sanz J. L., Cayón L., 2004, ApJ, 609, 22, arXiv:astro-ph/0310273